Sensorless Speed and Position Control of Synchronous Machines using Alternating Carrier Injection

Marco Linke, *Student Member*, Ralph Kennel, *Senior Member,* Joachim Holtz, *Fellow*

University of Wuppertal
Electrical machines and drives
http://www.ema.uni-wuppertal.de

Abstract — **High frequency carrier injection is a promising approach solving high performance sensorless drive demands. Position control at low and zero speed is only possible using anisotropic effects considered in high-frequency models. The usually open loop carrier signal injection is impacted by nonlinear inverter properties like the dead-time effect. This paper discusses the influence of the dead time effect on the carrier signal excitation comparing alternating and revolving injection principles. To overcome disturbing effects an alternating injection procedure is proposed using a predefined injection angle. The approach reduces the effects of the inverter distortion voltages.**
As a result it is possible to track even small saliencies typical for surface mounted permanent magnet synchronous machines. For processing the high frequency current for position estimation, there is no additional hardware necessary within a standard drives with field oriented control. The paper presents theoretical analysis and experimental results.

Index terms **— sensorless position control, carrier injection, dead-time effect,**

I. INTRODUCTION

I. A. High frequency carrier injection

Several proposals have been made to use estimation algorithms for speed detection and even for position detection of synchronous machines at low and zero speeds. Papers recently published indicate high frequency injection methods becoming more and more attractive [1, 4, 5]. In Surface Mounted Permanent Magnet Synchronous Machines (SMPMSM) the saliencies are small, because the magnets are distributed rather homogenously on the surface of the rotor. Therefore injection methods usually are not applied to this type of machines.
These machines, however, provide a small amount of anisotropy produced by saturation of the main flux. This paper describes a high-frequency injection scheme to control speed and position in Surface Mounted Permanent Magnet Synchronous Machines especially at low stator frequency and even at standstill. The high-frequency test signal is controlled to be in alignment with the anisotropy of the rotor - in this case with the saliency induced by saturation - resulting in an amplitude modulated space vector. A *synchronous tracking scheme* evaluates the anisotropy – this concept avoids complex demodulation algorithms which are sensitive to variations of machine parameters and additional saliencies neglected by the model.

The inverter dead-time effect represents the major carrier signal distortion. In chapter V these highly nonlinear effects are discussed. In revolving carrier systems an elliptical carrier voltage distortion can be observed leading to misinterpretations of the actual anisotropic machine properties reflected in the carrier current. For alternating carrier injection schemes a variation of the carrier injection angle has been analyzed to overcome the inverter dead-time effect, which has a strong impact on the high frequency carrier signal excitation. The approach bases on reducing the inverter distortions voltages by using the orthogonal estimation axis.

I. B. Alternating high frequency carrier injection schemes

Alternating carrier injection schemes are able to track reliably even small anisotropies. In differences to revolving carrier injection schemes the alternating carrier methods are able to decouple different saliency effects. This is due to the orientation of the orthogonal estimation axis according to the saliency aligned excitation axis [7]. The approach in [7] uses a so-called “in phase component isolator” (separating the anisotropy information). An adjusting procedure is suggested to compensate the degrading demodulation performance with increasing carrier phase lags due to inaccuracies of the inverter and measuring equipment.

In difference to [7] the method presented in this paper proposed a *phase sensitive rectifier* incorporating additionally *d*-axis current information to process an (online minimized) estimation error angle.

Alternating carrier injection with a displacement of $\pi/4$ with respect to the saliency axis [4], suffers from inverter carrier voltage harmonics generated by the dead time effect. This effect can be explained by analysing the current trajectory transition between two switching sectors.

II. ALTERNATING CARRIER INJECTION PRINCIPLE

The phase angle of an alternating carrier voltage vector $\boldsymbol{u}_c$ is kept in alignment with the estimated *d*-axis in the *dq*-rotor reference frame (Fig. 1). As a consequence, the modulation has almost no effect on the torque producing current component in the *q*-axis [11].

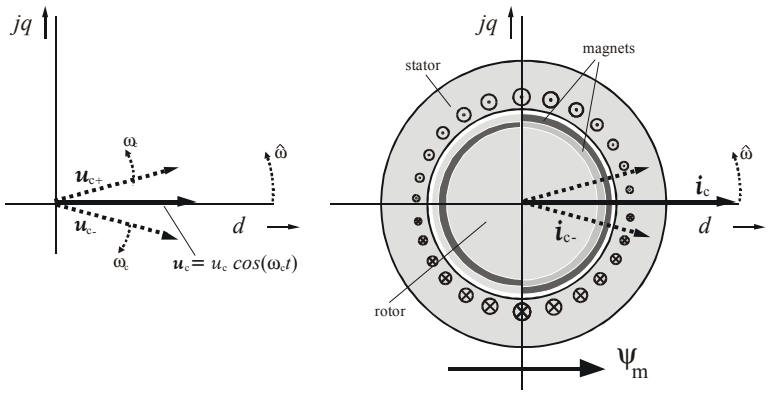

Fig.1: Resulting current signal $\boldsymbol{i}_c$ as a modulated space vectors in rotor coordinates

Based on this approach the superimposed carrier signal can be described in stator coordinates as follows

$$\boldsymbol{u}_c^{(S)} = u_c \cos(\omega_c t)\, e^{j\hat{\omega}t} . \qquad (2.1)$$

The carrier frequency ω_c is chosen around 2 kHz to obtain a fast response and to avoid interaction with the current control loop. As long as the estimated rotor position coincides with the real rotor position δ the test signal is a composition of two high frequency test signals as used in conventional high-frequency injection methods [2] but rotating in directions opposite to each other. As a result only the d-axis is excited by the carrier. The resulting high-frequency current $\boldsymbol{i}_c$ (response of the electromagnetic circuits to the injection voltage $\boldsymbol{u}_c$) is also in alignment with the main flux. Like the voltage the current can be also decomposed to a positive and negative sequence component, $\boldsymbol{i}_{c-}$ and $\boldsymbol{i}_{c+}$ respectively (Fig. 1). The amplitude of $\boldsymbol{i}_c$ varies sinusoidally with time. A small misalignment between the real and the estimated rotor position produces an additional high frequency component

$$\boldsymbol{i}_c^{(\hat{\delta})} = \frac{u_c}{l_d l_q} \sin(\omega_c t) \left[l_d + (l_q - l_d)\, e^{-j(\hat{\delta}-\delta)} \right] \qquad (2.2)$$

which can be detected to feed a rotor saliency tracking algorithm which is sensitive even to the small anisotropies of SMPMSMs [11]. The current signal (2.2) is not used to estimate the rotor position by calculations. It serves as an error signal that is minimized by the tracking scheme in the next sampling cycle.

III. ESTIMATIN OF THE ANISOTROPY

The new method generates a positive as well as a negative current sequence component, both containing information about the rotor position. The injected carrier voltage

$$\boldsymbol{u}_c^{(S)} = u_c \cos(\omega_c t)\, e^{j\hat{\delta}_a} \qquad (3.1)$$

is always in alignment with the estimated position of the anisotropy (estimated values are marked with a hat ^):

$$\hat{\delta}_a = \hat{\omega}_a t . \qquad (3.2)$$

The anisotropy in a SMPMSM is mainly based on the saturation effect of the main flux; it rotates with the same frequency ω as the rotor. In difference to the field oriented system the subscript $_a$ generally indicates an anisotropy-aligned coordinate system. Both coincide in the case of surface mounted PMSM. A transformation of the carrier voltage to field coordinates is done by multiplying equation (3.1) by $e^{-j\delta}$. This leads to

$$\boldsymbol{u}_c^{(F)} = u_c \cos(\omega_c t)\, e^{j(\hat{\delta}-\delta)} . \qquad (3.3)$$

The differential stator equation can be represented as follows:

$$\boldsymbol{u}_c^{(F)} = u_c \cos(\omega_c t)\, e^{j(\hat{\delta}-\delta)} = \boldsymbol{l}_\sigma^{(F)} \frac{d\,\boldsymbol{i}_c^{(F)}}{dt} \qquad (3.4)$$

Stator resistance, induced voltage and cross coupling of the currents are neglected in the differential stator equation [11]. This is only permitted if the carrier frequency ω_c is much higher than the fundamental frequency.

The real field angle δ is the unknown variable in this equation. The solution in field coordinates of (3.4) is

$$\boldsymbol{i}_c^{(F)} = \frac{u_c}{\omega_c} \sin\omega_c t \left(\frac{1}{l_{\sigma d}} \cos(\hat{\delta}-\delta) + j \frac{1}{l_{\sigma q}} \sin(\hat{\delta}-\delta) \right) . \qquad (3.5)$$

Equation 3.5 can be discussed as follows: the carrier current amplitude $|\boldsymbol{i}_c|$ increases proportionally to the carrier voltage $\boldsymbol{u}_c$ and decreases with increasing carrier frequency. Moreover, the carrier current component i_{cq} is directly proportional to the angle error Δδ.

This offers an effective way to demodulate the rotor position information. The *sin*-function from (3.5) behaves proportion-

ally to the angle error Δδ. Hence, the next processing cycle is used to correct the direction of carrier signal.

IV. SENORLESS CONTROL APPROCH

IV. A. Demodulation of the carrier current

Using high frequency injection methods for sensorless control, the signal demodulation algorithm requires high performance in signal processing. To reduce the calculation effort, the high-frequency current $\boldsymbol{i}_c$ (3.5) is transferred to a reference frame in a negative direction at approximate carrier frequency. This is done by

$$\boldsymbol{i}_c^{(\omega_c t+\hat{\delta})} = \boldsymbol{i}_c^{(S)}\, e^{-j(\omega_c t+\hat{\delta})} \tag{4.1}$$

This transformation generates a high frequency current signal that is easy to demodulate without referring to machine parameters. Assuming the remaining negative sequence current components of $\boldsymbol{i}_c$ are rejected by a low pass filter, transformation (4.1) applied to the current signals (3.5) results in

$$\boldsymbol{i}_p^{(\omega_c t+\hat{\delta})} = u_c \;\; \frac{1}{j4\,\omega_c\, l_{\sigma d}\, l_{\sigma q}} \begin{bmatrix} (l_{\sigma d}+l_{\sigma q}) \\ -(l_{\sigma d}-l_{\sigma q}) e^{j(2\delta-2\hat{\delta})} \end{bmatrix}. \tag{4.2}$$

It can easily be separated because it is transformed by (4.1) to about twice the carrier frequency.

Equation 4.2 illustrates the current response containing the useful information about the misalignment of the estimated field angle with reference to the real field angle. It is used as an error estimation angle

$$\Delta\delta = \delta - \hat{\delta}\,. \tag{4.3}$$

The current response is further simplified to reduce processing power necessary for demodulation. In the case of small error estimation angles the current response is:

$$\boldsymbol{i}_p^{(\omega_c t+\hat{\delta})} = u_c \;\; \frac{1}{4\,\omega_c\, l_{\sigma d}\, l_{\sigma q}} \begin{bmatrix} -j(l_{\sigma d}+l_{\sigma q}) \\ -(l_{\sigma d}-l_{\sigma q})\, 2\,\Delta\delta \end{bmatrix} \tag{4.4}$$

This equation shows the real component of the current response in the reference frame according to (4.1) being proportional to the error angle Δδ. This is used to track the field angle by a closed loop tracking system (Fig. 2).

IV. B. Sensorless position control of SMPMSM

As discussed in chapter IV.A, a high sophisticated demodulation of the carrier response can be replaced by tracking the error estimation signal (4.3). It is possible to generate a calculation quantity representing the misalignment Δδ between the estimated field angle and its real value, (4.4). Tracking an error signal is robust against noise and measurement tolerances e.g. the limited resolution of analog to digital converters in drive controllers. As the *estimated field error angle* Δδ is evaluated in the proposed method instead of the absolute *field angle* itself, the resolution of the high frequency current signal $\boldsymbol{i}_c$ is less critical. Furthermore, the error signal Δδ is changing only slowly in comparison to the sample frequency.

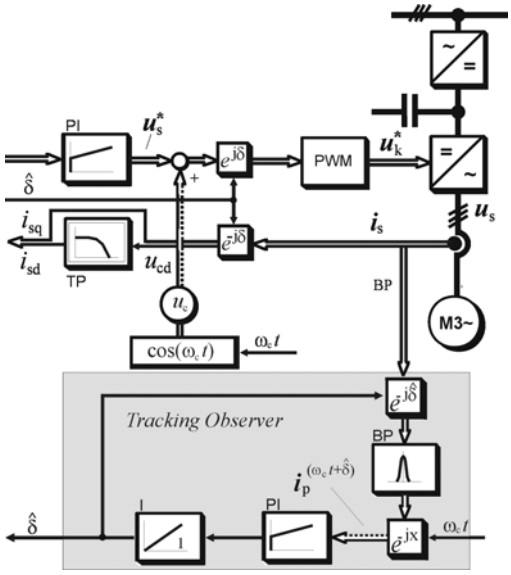

Fig.2: Signal flow graph of the field angle estimation scheme based on the proposed method

The signal flow graph in Figure 2 illustrates the basic structure of the proposed sensorless scheme. The positive sequence current has a real component proportional to the error angle Δδ (4.4). This signal is sampled with the sampling frequency of the current control loop. The following PI-controller feeds a controlled oscillator to create the estimated field angle. This results in a closed loop structure that corrects the field angle stepwise by each sampling cycle. Hence, a high sampling frequency ensures good and dynamical fast alignment with field axis. The disturbances of the acquired signal are low, thus permitting operation at low carrier amplitudes. The prominent advantage is the tracking observer not depending on any machine parameters.

To establish narrow filter characteristics, the current $\boldsymbol{i}_c$ (Fig. 2) is transformed to the estimated field coordinate system by

$$\boldsymbol{i}_c^{(\hat{\delta})} = \boldsymbol{i}_c^{(S)}\, e^{-j(\hat{\delta})}\,. \tag{4.5}$$

This transformation results only in current components of carrier frequency ω_c. This allows using narrow band filters that rejecting all frequencies except the carrier frequency, which is essential to estimate small saliencies.

IV. C. Experimental results

The experimental results are obtained using a commercial 6-pole SMPMSM servo drive with 1.2 kW rated power.

The estimated position $\hat{\delta}$ is used as a feedback signal for field oriented control. The central track of the diagram in Figure 3 represents the position error $\Delta\hat{\delta}$ between the measured position δ and the estimated position $\hat{\delta}$ (increased scale). The switching frequency is 8 kHz, the carrier frequency is 2 kHz with a peak carrier current $i_{c,max}$ of 200 mA. The current is processed using the same 12-Bit A/D converter also used for sensing the fundamental currents.

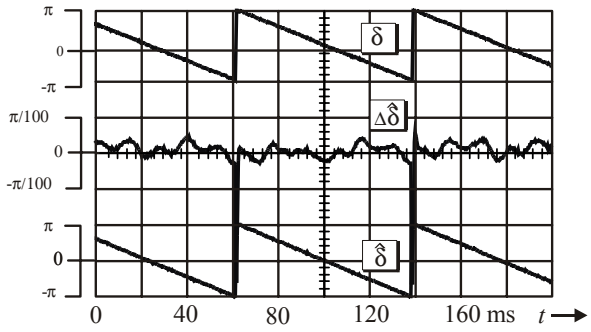

Fig. 3: Experimental results: rotor position δ and corresponding estimated variables $\hat{\delta}$, $\Delta\hat{\delta}$

V. DEAD-TIME EFFECT ON CARRIER EXICITATION

V.A. Modeling of the Dead-time effect

The major distortions of the inverter output are caused by an interlock time T_d, preventing a temporary short circuit of the DC link when using a voltage source inverter. The interlock time T_d is typically higher than the turn off time of the individual IGBT. During the interlock time the upper and lower power switches are turned off, therefore each half bridge output potential is determined by the state of the freewheeling diodes and hence by the polarity of the load current [6]. This situation is valid for fundamental stator currents as well as for high frequency carrier currents.

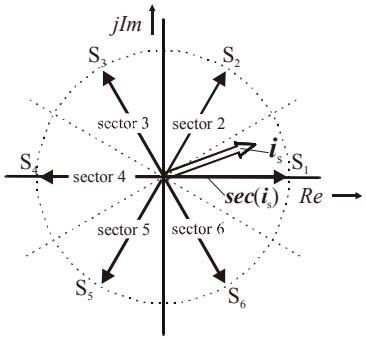

Fig.4: Definition of the six distortion voltage vectors $\mathbf{S}_i$ according to each stator current sector

Figure 4 shows six distortion voltage vectors $\boldsymbol{S}_i$ located in a complex plane according to the stator current $\boldsymbol{i}_s$ [6]. It can be seen that each error voltage have the same amplitude but they are displaced to each other by 60 degrees phase angle. The six sectors determine the appropriate error voltage phase angle by

$$\boldsymbol{sec}(\boldsymbol{i}_s) = \frac{2}{3}\left[a^0\ sign(i_{sa}) + a^1\ sign(i_{sb}) + a^2\ sign(i_{sc})\right]. \quad (5.1)$$

The variables $i_{s,a,b,c}$ are the respective stator phase currents, $a = e^{j2\pi/3}$ is the vector rotator and *sign* represents the polarity of the respective phase current (a detailed description of this scheme can be found in [6]). This justifies the definition of a complex error voltage vector .

$$\boldsymbol{u}_{er} = \frac{T_d - T_{off}}{T_0}\,\boldsymbol{sec}(\boldsymbol{i}_s) = \Delta u\ \boldsymbol{sec}(\boldsymbol{i}_s) \quad (5.2)$$

The normalized error voltage vector $\boldsymbol{u}_{er}$ is a nonlinear function of the stator current $\boldsymbol{i}_s$ and is mainly proportional to the effective IGBT off-states $T_d - T_{off}$ [6]. The six error voltages result in a sixth harmonic of the stator current.

V.B. Distortion of rotating Carrier Injection

The revolving carrier excitation represents a widely known method of sensorless control [2]. Usually all high frequency carrier methods are arranged as an open loop injection scheme, assuming inverter linearity. The distortion phenomena caused by the inverter dead-time is normally neglected, although it can lead to serious problems [10].

The fundamental distortion model discussed above is also valid for high frequency injection. However the influence on the carrier signal is different to the influence on the fundamental states. The high frequency sector transition, inherent to this signal class, lead to high harmonic error voltages $\boldsymbol{u}_{er}$.

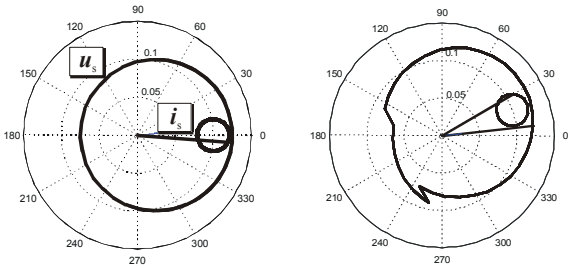

a) α=0 b) α=20

Fig.5: Stator voltage $\boldsymbol{u}_s$ and current trajectory $\boldsymbol{i}_s$, applying a rotating carrier voltage $\boldsymbol{u}_c = u_c e^{j\omega_c t}$ and a constant fundamental voltage $\boldsymbol{u}_{s1} = u_{s1} e^{j\alpha}$ (simulation)

For symmetrical reasons the following discussion is focused on sector one and two only. All experimental results in this chapter are taken using an isotropic machine. Therefore they solely present the undesired modulation effect of the inverter nonlinearity without any impact of the other effects.

Figure. 5 presents the stator and voltage trajectory incorporating the dead time-effect, as typically present in sensorless carrier methods. The usually larger and slowly varying fundamental current $\boldsymbol{i}_s$, is emulated (for illustration purposes) as a constant DC current with predefined stator angle. The superposition of a small high frequency carrier current and a large fundamental current leads to characteristical sector transitions. The high frequency voltage vector $\boldsymbol{u}_c$ is superimposed to the fundamental one, resulting in a high frequency current trajectory $\boldsymbol{i}_c$ shown by the fundamental DC current summing up to the stator current $\boldsymbol{i}_s$ (see Fig 5).

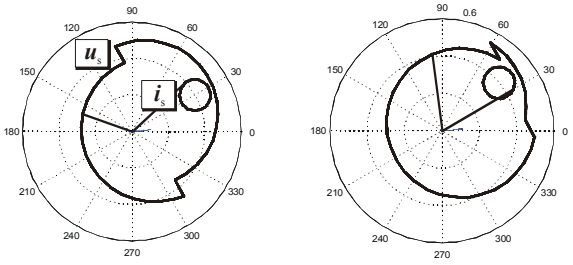

a) α=30 b) α=40

Fig.6: Stator voltage and current trajectory $\boldsymbol{u}_s$, $\boldsymbol{i}_s$, applying a rotating carrier voltage $\boldsymbol{u}_c = u_c e^{j\omega_c t}$ and a fundamental constant voltage $\boldsymbol{u}_{s1} = u_{s1} e^{j\alpha}$ (simulation)

As the high frequency current touches the sector boundary defined in Fig. 4, the high frequency voltage gets distorted by an error voltage $\boldsymbol{u}_{er}$ (see Fig. 5b). The error voltage is deducible considering equation (5.1). A strong elliptical modulation effect of the carrier voltage trajectory $\boldsymbol{u}_c$ is visible. It depends directly on the high frequency current transition and is strongly nonlinear. Therefore the maximum influence between both sectors can be expected at 30 degrees fundamental current angle.

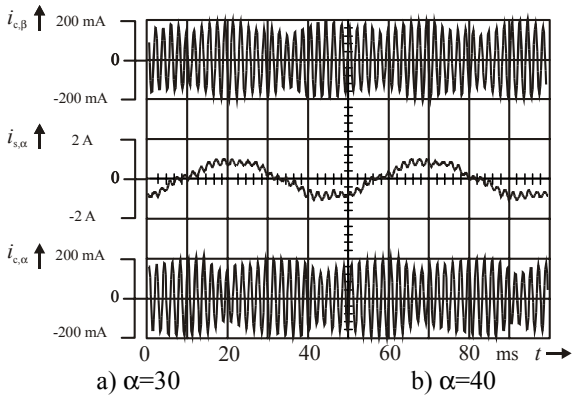

a) α=30 b) α=40

Fig.7: Measured distortions of the filtered carrier current components $i_{c\alpha}$ $i_{c\beta}$ resulting from the dead-time effect, (f_s = 6 kHz, T_d =5 µs)

Figure 6 points out the elliptical modulation effect considering the fundamental current phase angles α of 30 and 40 degrees. The maximum carrier voltage distortion takes place at 30 degrees fundamental current phase angle as expected. Consequently the elliptical carrier distortion bases on an error voltage $\boldsymbol{u}_{er}$ with carrier frequency ω_c, hence not eliminable by any filter.

Figure 7 illustrates the consequences of a distorted carrier voltage trajectory (increased dead-time for better illustration). The carrier current gets modulated cyclically whenever one of the fundamental phase current components passes zero. This modulation effect is hardly separable from desired anisotropic machine modulation effects because of the frequency spectra are very close together.

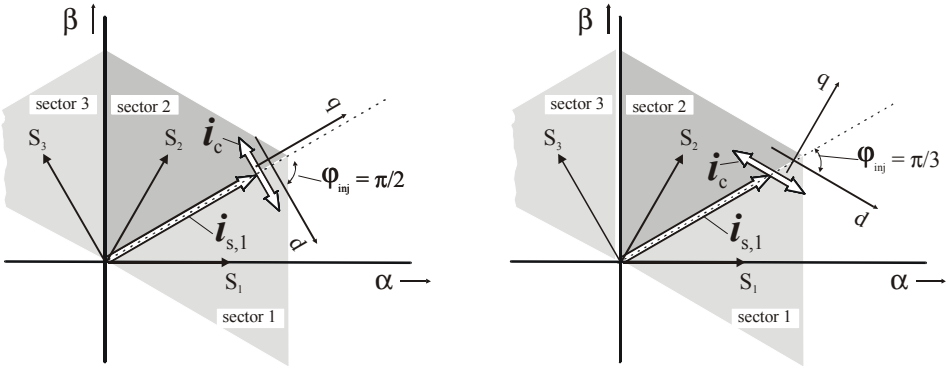

a) injection angle $\varphi_{inj} = \pi/2$ b) injection angle $\varphi_{inj} = \pi/3$

Fig. 8: High frequency carrier current transition during sector changes with different injection angles φ_{inj} according to the fundamental stator current $\boldsymbol{i}_{s1}$

V.C. Distortion of alternating carrier injection

Small saliencies require a highly sensitive estimation method, which must be robust against parasitic anisotropies like inverter clamping effects. Results shown below make clear that the orientation of the injected alternating voltage according to [11] provides an important additional degree of freedom. This can be understood by studying the sector change in Fig. 8.

The dead time effect generates six different error voltage vectors $\mathbf{S}_1$-$\mathbf{S}_6$ depending on the actual stator current $\boldsymbol{i}_s$. Regarding sector 1 and 2 as an example, it is obvious, that the high frequency alternating current trajectory determines a high frequency error vector transition during the sector change (Fig. 8). The current trajectory, however, depends directly on the injection angle φ_{inj} of the high frequency signal according to the fundamental current $\boldsymbol{i}_{s1}$. This results in an alternating high frequency voltage distortion signal with carrier frequency. In the case of Fig. 8 the error voltage $\boldsymbol{u}_{er}$ can be decomposed into a constant DC-voltage term according to the mean value of both distortion voltages $\mathbf{S}_1$,$\mathbf{S}_2$ (neglecting the variation of the DC-term during one fundamental period) and the alternating term (at carrier frequency) according to the difference of $\mathbf{S}_1$,$\mathbf{S}_2$.

$$\boldsymbol{u}_{er}^{(S)} = \Delta u \left(\frac{\boldsymbol{S}_1 + \boldsymbol{S}_2}{2} + \frac{\boldsymbol{S}_1 - \boldsymbol{S}_2}{2}\ rect(\omega_c t) \right) \tag{5.3}$$

With respect to its frequency the alternating term (*rect*) is not separable by filters. Therefore the impact on the carrier signal can be reduced only under the following three conditions:

- minimizing the *inverter interlock time*
- minimizing the transition time between two sectors
- a properly used carrier injection angle φ_{inj}

The first two methods are not under the control of the design engineer and therefore obviously less applicable. The last point can be used to determine a predefined injection angle φ_{inj} to minimize the impact of the distortion voltage $\boldsymbol{u}_{er}$.

The distortion voltage observed in a synchronous *dq*-reference frame as in Fig. 8 depends on the injection angle φ_{inj} and can be calculated according to (5.3) by vector transformation. Fig. 9 illustrates the voltage distortion in the *d*- and *q*-component at different injection angles.

It is important to realise that there exists a periodically modulated *q*-axis carrier voltage u_{cq} even when the high carrier excitation is injected in the *d*-axis only. The distortion voltage component $u_{err,q}$ is strongly increased depending on the injection angle. A correct high frequency carrier current response $i_{c,q}$ modulated by machine anisotropies can therefore only be expected for undistorted voltage carrier components u_{cq}. This is nearly guaranteed for an injection angle of

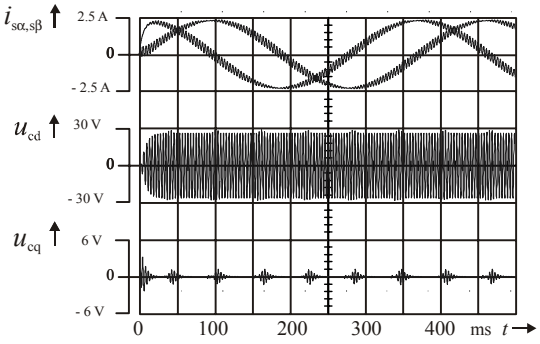

a) Injection angle $\varphi_{inj} = \pi/2$

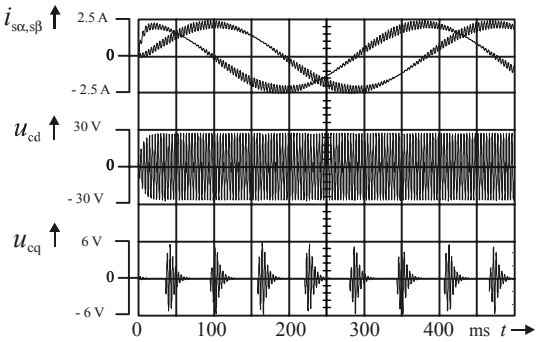

b) injection angle $\varphi_{inj} = \pi/3$

Fig. 9: Distortion of the high frequency carrier voltage components u_{cq}, u_{cd} during one fundamental period (due the inverter dead time effect) at different injection angles φ_{inj} (simulation)

$\varphi_{inj} = \pi/2$. (Carrier excitation with the injection angle $\varphi_{inj} = 0$ theoretically also results in a minimum distortion. But experiments confirm that this can hardly be realized.)

The distortion effect of the error voltage $\boldsymbol{u}_{er}$ influences the carrier voltage components u_{cq}, u_{cd} depending on the injec-

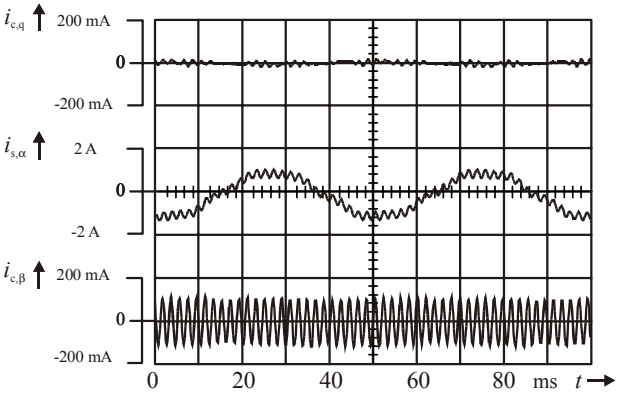

Fig.10: Measured distortions of the filtered carrier current components i_{cd} i_{cq} resulting from the dead-time effect, (f_s = 6 kHz, T_d =5 µs, $\varphi_{inj} = \pi/2$)

tion angle. However, the relative distortion of the *d*-component is very small because it coincides with the main excitation direction. The *q*-component, generally used for anisotropic machine identification, is highly sensitive to voltage distortions. Therefore distortions caused by inverter nonlinearities should be avoided in this axis by means of proper injection angles φ_{inj} .

Figure 10 confirms the theoretical results concerning the minimum distortion effect in the *q*-component using an injection angle of $\varphi_{inj} = \pi/2$. Even though there is a modulation of the *d*- carrier current the *q*-carrier current remains nearly unaffected.

Under load conditions the fundamental machine current $\boldsymbol{i}_s$ is perpendicular to the main field (no field weakening) and the carrier current is aligned with the main field axis. Therefore the injection angle is close to $\pi/2$. Hence the processed *q*-carrier current i_{cq} (Fig. 2) is almost not affected by the inverter dead time effect. This situation provides a high accuracy in rotor position estimation visualised in Figure 3.

VI. CONCLUSION

This paper presents an improved sensorless control algorithm for Surface Mounted Permanent Magnet Synchronous Machines using high-frequency voltage injection. The method is suitable for reluctance machines and permanent magnet machines with buried magnets, but it is especially designed to track small saliencies and to detect the small differences in rotor anisotropy provided by synchronous motors with surface mounted permanent magnets. The position estimation method is independent of machine parameters as only a position error is estimated by a tracking scheme.

Special attention is given to the inverter nonlinearities affecting the carrier signal. Hence a special injection scheme using predefined injection angles is suggested. This results in a minimum carrier distortion with reference to the orthogonal estimation axis. Experimental results verify inverter nonlinearities being minimized by a proper choice of the injection angle.

REFERENCES

1. J. Holtz, Sensorless Position Control of Induction Motors - an Emerging Technology, IEEE Transactions on Industrial Electronics, Vol. 45, No. 6, December 1998.
2. Robert D. Lorenz, Sensorless Drive Control Methods for Stable, High Performance, Zero Speed Operation, International Conference on Power Electronics and Motion Control- EPE-PEMC, Kosice 2000.
3. J.K Ha, S.K. Sul, K. Ide, I. Murokita, K. Sawamura, Physical Understanding of High Frequency Injection Method to Sensorless Drives of an Induction Machine, IEEE-IAS 2000, Conference Record of the 2000 IEEE Ind. Appl. Conference, Vol.4
4. J.K. Ha, S.K. Sul, Sensorless Field-Orientation Control of an Induction Machine by High-Frequency Signal Injection, IEEE Tran. On Ind. Appl., Vol. 35. No.1, Jan./Feb. 1999
5. A.Consoli, F. Russo, A. Testa, Low- and Zero-Speed Sensorless Control of Synchronus Reluctance Motors, IEEE Trans. On Ind. Appl., Vol.35, No.5, Sept./Oct. 1999,pp.1050-1050
6. J. Holtz: Pulsewidth Modulation for Power Converters, *Proceedings of the IEEE*, Vol. 82, No. 8, Aug. 1994, pp. 1194-1214.
7. P.L. Jansen, Sensorless Rotor Tracking of Induction Machines with Asymmetrical Rotor Resistance, Patent Number: 6,1237,258, May 30, 2000, USA,
8. L.A.S. Ribeiro, M.W. Degner, F. Briz, and R.D. Lorenz, Comparing Carrier Frequency Current and Voltage Injection for the Estimation of Flux, Position, and Velocity in Sensorless AC Drives, *Proceedings of IEEE-IAS Conf.* , Oct. 12-16, 1998, St. Louis, pp. 452-459.
9. N. Teske**,** G. M. Asher**,** M. Sumner, and K. J. Bradley: Suppression of Saturation Saliency Effects for the Sensorless Position Control of Induction Motor Drives under Loaded Conditions, *IEEE Transactions on Industrial Electronics*, vol. 47, no. 5, pp. 1142 - 1150, Oct. 2000.
10. N. Teske**,** G. M. Asher**,** K. J. Bradley, and M. Sumner: Analysis and Suppression of Inverter Clamping Saliency in Sensorless Position Controlled Induction Machine Drives," *Conf. Rec. IEEE-IAS Annual Meeting, no. 36*, Chicago, USA, Sept./Oct. 2001
11. M. Linke, R. Kennel, J. Holtz: Sensorless position control of Permanent Magnet Synchronous Machines without Limitation at Zero Speed, *28th Annual Conference of the IEEE Industrial Electronics Society IECON'02,* Sevilla/Spain, Nov. 5-8, 2002.